doi:10.1016/j.jmb.2006.10.092 J. Mol. Biol. (2007) 366, 1437–1446

JMB

Available online at www.sciencedirect.com

ScienceDirect

ELSEVIER

Crystal Structures of Human IPP Isomerase: New Insights into the Catalytic Mechanism

Cheng Zhang[1,2], Lin Liu[1,2], Hang Xu[1], Zhiyi Wei[1,2], Yanli Wang[1] Yajing Lin[1] and Weimin Gong[1,2]*

[1]*National Laboratory of Biomacromolecules Institute of Biophysics Chinese Academy of Sciences Beijing, 100101 PR China*

[2]*School of Life Sciences University of Science and Technology of China Hefei, Anhui, 230026 PR China*

**Corresponding author*

Type I isopentenyl diphosphate (IPP): dimethylally diphosphate (DMAPP) isomerase is an essential enzyme in human isoprenoid biosynthetic pathway. It catalyzes isomerization of the carbon-carbon double bonds in IPP and DMAPP, which are the basic building blocks for the subsequent biosynthesis. We have determined two crystal structures of human IPP isomerase I (hIPPI) under different crystallization conditions. High similarity between structures of human and *Escherichia coli* IPP isomerases proves the conserved catalytic mechanism. Unexpectedly, one of the hIPPI structures contains a natural substrate analog ethanol amine pyrophosphate (EAPP). Based on this structure, a water molecule is proposed to be the direct proton donor for IPP and different conformations of IPP and DMAPP bound in the enzyme are also proposed. In addition, structures of human IPPI show a flexible N-terminal α-helix covering the active pocket and blocking the entrance, which is absent in *E.coli* IPPI. Besides, the active site conformation is not the same in the two hIPPI structures. Such difference leads to a hypothesis that substrate binding induces conformational change in the active site. The inhibition mechanism of high Mn^{2+} concentrations is also discussed.

Keywords: IPP isomerase; substrate analog; conformation change; inhibition

Introduction

Isoprenoid biosynthesis is an important biological pathway. The products of this pathway are extraordinarily various, among which more than 23,000 natural products have been characterized, including many essential small molecules such as sterols, carotenoids, ubiquinones etc.[1,2] In addition, several GTPases that are needed to be prenylated are related to this pathway.[2,3] The enzymes involved in this pathway are of great interest for drug design. For example, Statins, inhibitors of HMG CoA reductase, are widely used as cholesterol-lowering drugs.

Isopentenyl pyrophosphate (IPP): dimethylallyl pyrophosphate (DMAPP) isomerase (IPP isomerase, IPPI) is an essential enzyme in the isoprenoid biosynthetic pathway. It catalyzes isomerization of the carbon-carbon double bonds in IPP and DMAPP (Figure 1(a)), which are the basic building blocks in the following head-to-tail condensation reactions that produce numerous isoprenoid products.[4] In fact, there are two types of IPP isomerase known in nature. Type I IPP isomerase has been characterized long ago[5] and exists in most species.[6] Type II IPP isomerase was recently discovered in Archaea and some eubacteria.[6] For human, some compounds belonging to phosphoantigens, which are γδ T cell antigens of clinical interests,[7–9] are proved to be inhibitors of type I IPP isomerase.[10,11]

The reaction catalyzed by Type I IPP isomerase involves a stereoselective antarafacial transposition of hydrogen.[12] Many studies have been carried out in order to understand the mechanism of isomerization. Protonation/deprotonation mechanism was supported by many experiments and a carbocation intermediate was proposed[13–15] (Figure 1(a)). It was also proven by mutagenesis and other experiments that Cys139 and Glu207 are catalytically critical

Abbreviations used: IPP, isopentenyl diphosphate; DMAPP, dimethylally diphosphate; IPPI, IPP isomerase; hIPPI1, crystal structure of human IPPI that belongs to space group $P2_12_12_1$; hIPPI2, crystal structure of human IPPI that belongs to space group $P1$; hIPPI2_A and hIPPI2_B, two monomers in one asymmetry unit of hIPPI2; EAPP, ethanol amine pyrophosphate; NIPP, *N*,*N*-dimethyl-2-amino-1-ethyl diphosphate.

E-mail address of the corresponding author: wgong@ibp.ac.cn

0022-2836/$ - see front matter

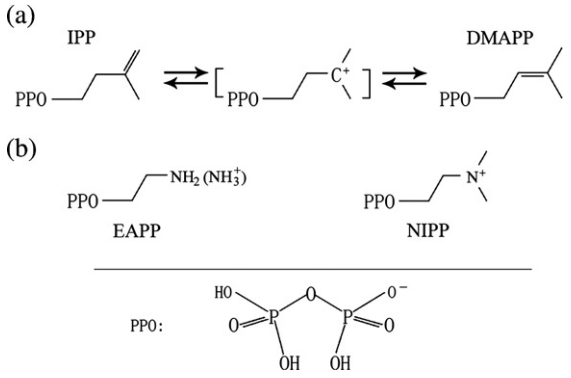

Figure 1. (a) Reaction catalyzed by type I IPP isomerase. IPP, DMAPP and the carbocationic intermediate are shown. (b) Structural formula of EAPP and NIPP.

residues in yeast,[16,17] corresponding to Cys67 and Glu116 in *Escherichia coli* and Cys86 and Glu148 in human.

Crystal structures of *E.coli* Type I IPP isomerase (*E.coli* IPPI) and its complexes bound with different substrate analogs have been extensively studied. Based on these structures, detailed mechanism has been proposed and supported by mutagenesis studies.[11,18–22] However, sequence alignment shows that eukaryotic Type I IPP isomerases contain several inserted fragments and an extra N-terminal region. Therefore, whether *E. coli* IPP isomerase structures and the proposed mechanism are universally applicable to eukaryotic IPP isomerases remains unclear, because no IPP isomerase structure from other organisms is available. More importantly, in order to develop potential cholesterol lowering drugs[6] or phosphoantigens[10,11] against human diseases, the knowledge of structure and catalytic mechanism of human IPP isomerase is necessary. Here we report crystal structures of human IPP isomerase in two different crystal forms, one of which is bound with a substrate analog.

Results

Overall structure

The statistics of structure refinements of hIPPI are summarized in Table 1. The native hIPPI and the Se-Met hIPPI bound with a substrate homolog are referred to hIPPI1 and hIPPI2, respectively. There is one monomer per asymmetric unit in hIPPI1 and two monomers per asymmetric unit in hIPPI2, named hIPPI2_A and hIPPI2_B.

The overall structures of hIPPI1 and hIPPI2 are similar to that of *E.coli* IPPI except for some differences discussed below. The core structure of hIPPI folds into a compact globular domain of α/β fold as *E.coli* IPPI, but with some insertions at the molecular surface (Figure 2(a)). Compared to *E. coli* IPPI, the extra C-terminal peptide of hIPPI folds into an extra α-helix (α7) followed by a β-strand (βJ) (Figures 2(a) and 3). It was reported that the last three C-terminal residues YRM would be peroxisomal targeting signal residues.[23] These three residues are located in βJ, which forms a parallel β-sheet with βG. The side-chains of Tyr225 and Met227 are involved in hydrophobic interactions between βJ and the core structure, while the side-chain of Arg226 forms a hydrogen bond with Glu26.

More interestingly, a substrate analog is found in the active pocket in hIPPI2 crystal. According to the annealing omit F_o–F_c electron density map (Figure 4(a) and (b)), this molecule was assigned as ethanol amine pyrophosphate (EAPP), a natural component of *E. coli* cell wall that had been found in the structure of *E. coli* ferric hydroxamate uptake protein bound with lipopolysaccharide (LPS) (PDB code 2FCP). The EAPP molecule should have been co-purified with the recombinant hIPPI protein and leads to insights of the catalytic mechanisms.

In the available substrate analog binding structures of *E.coli* IPPI, there are two metal ion binding

Table 1. Statistics of data collection and model refinement

Data set	hIPPI1	hIPPI2
Space group	$P2_12_12_1$	$P1$
Unit cell parameters	a=55.0 Å, b=63.0 Å, c=74.2 Å	a=41.4 Å b=43.1 Å c=70.5 Å α=80.3° β=90.0°, γ=68.0°
	α=β=γ=90°	
Resolution range (Å)	50–1.60 (1.66–1.60)	50–2.0 (2.07–2.00)
No. of total reflections	587,258	567,543
No. of unique reflections	33,566 (2355)	56,531(5231)
I/σ	32.2 (3.5)	18.2 (3.8)
Completeness (%)	96.3 (68.7)	94.1 (87.0)
R_{merge} (%)[a]	6.9 (37.3)	9.8 (46.4)
R_{work}(%)[b]/R_{free}(%)[c]	17.3/20.3	22.0/26.2
B factors (Å^2)		
Main-chain atoms	15.9	39.6 (hIPPI2_A) 39.0 (hIPPI2_B)
Side-chain atoms	17.2	41.2 (hIPPI2_A) 40.8 (hIPPI2_B)
Water molecules	29.2	40.2
Mn^{2+d}	13.2	29.5 (hIPPI2_A) 31.5 (hIPPI2_B)
EAPP[e]	–	36.0 (hIPPI2_A) 34.8 (hIPPI2_B)
Ramachandran plot		
Most favored regions (%)	87.8	88.2
Additional allowed regions (%)	12.2	11.8
RMSD of bonds length (Å)	0.008	0.013
RMSD of bond angles (deg.)	1.1	1.3

Numbers in parentheses represent the value for the highest resolution shell.

[a] $R_{merge}=\sum|I_i-I_m|/\sum I_i$, where I_i is the intensity of the measured reflection and I_m is the mean intensity of all symmetry-related reflections.

[b] $R_{work}=\sum||F_{obs}|-|F_{calc}||/\sum|F_{obs}|$, where F_{obs} and F_{calc} are observed and calculated structure factors, respectively.

[c] $R_{free}=\sum_T||F_{obs}|-|F_{calc}||/\sum_T|F_{obs}|$, where T denotes a test data set of about 5% of the total reflections randomly chosen and set aside prior to refinement.

[d] This Mn^{2+} refers to the one coordinated to His40, His51, His88, Glu146 and Glu148 in both structures of human IPPI.

[e] The substrate analog bound only in hIPPI2.

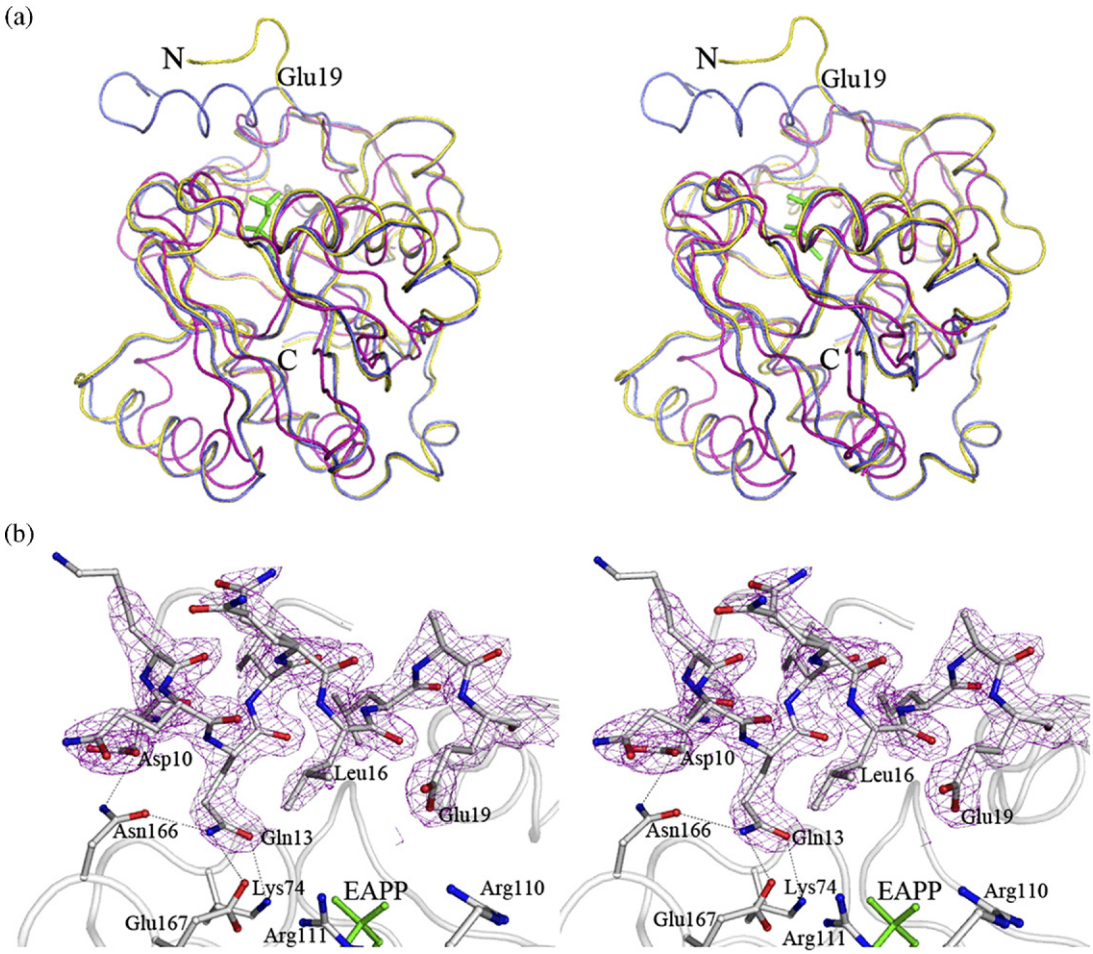

Figure 2. (a) Stereo view of superimposition of hIPPI1, hIPPI2_A and *E.coli* IPPI (PDB code 1NFS). hIPPI1 is colored in yellow. hIPPI2_A is colored in blue. *E.coli* IPPI is colored in magenta. EAPP bound in human IPPI2_A is colored in green. (b) Stereo view of the N-terminal α-helix in hIPPI2_A. The electron density map ($2F_o$–F_c map) of residues Asp10 to Glu19 is colored in purple and is contoured at 1.5σ. Hydrogen bonds Asp10 OD2 to Asn166 ND2, Gln13 OE1 to Lys74 NE, Gln13 NE2 to Asn166 OD1 and Glu167 OE2 are shown as black broken lines. EAPP is colored in green. Figures 2, 4 and 5 were prepared using PyMol [http://www.pymol.sourceforge.net].

sites.[19–21] The one required for catalysis exhibits a distorted octahedral coordination geometry involving His25, His32, His69, Glu114 and Glu116. The metal ion was assigned as Mn^{2+}[18] or Zn^{2+},[22,24] and it seemed that the *E coli* enzyme might prefer Zn^{2+} for this site.[22,24] Another metal ion binding site participates in substrate binding and was assigned as Mg^{2+}.[20–22] In both of the human IPPI structures, the catalytically essential metal ion is presented in a bipyramid coordination with His40, His51, His88, Glu146 and Glu148, similar to *E. coli* IPPI. This metal ion was assigned as Mn^{2+} in hIPPI1 and as Mg^{2+} in hIPPI2 according to the anomalous diffraction signal and metal ions added in the expression media and crystallization solutions (Figure 5(b)).

The N-terminal region

Although the core structures in the two crystal forms of human IPPI are highly similar, significant conformational variations are observed in the N-terminal region (Figure 2(a)). In hIPPI1, the N-terminal 12 residues seem to be disordered with no clear electron density. Residues Gln13 to Glu19 exist as a random coil. The active pocket is in an open state.

However in hIPPI2, where an EAPP molecule is bound in the active pocket, the N-terminal residues (Ile4 to Glu19 in one monomer and His8 to Glu19 in the other in hIPPI2) show clear electron density with Asp10-Glu19 folding into an α-helix located over the active pocket (Figure 2(b)). A number of hydrogen bonds: Asp10 OD2 to Asn166 ND2, Gln13 OE1 to Lys74 NE, Gln13 NE2 to Asn166 OD1 and Glu167 OE2, are formed between the N-terminal α-helix and the core structure (Figure 2(b)). Also, hydrophobic interactions formed by Leu9, Val14, Leu17, Leu41, Ile75, Ile143, and Trp144 also help to stabilize the N-terminal α-helix. In this situation, the active pocket is closed by the N-terminal peptide, especially by the side-chains of Gln13, Leu16 and Glu19. This substrate-induced open-closed mechanism was not observed in *E. coli* IPPI.

Compared to *E.coli* IPPI, extra N-terminal regions are widely observed in eukaryotic IPP isomerases (Figure 3). Residues Asp10, Gln13 and Leu17, which

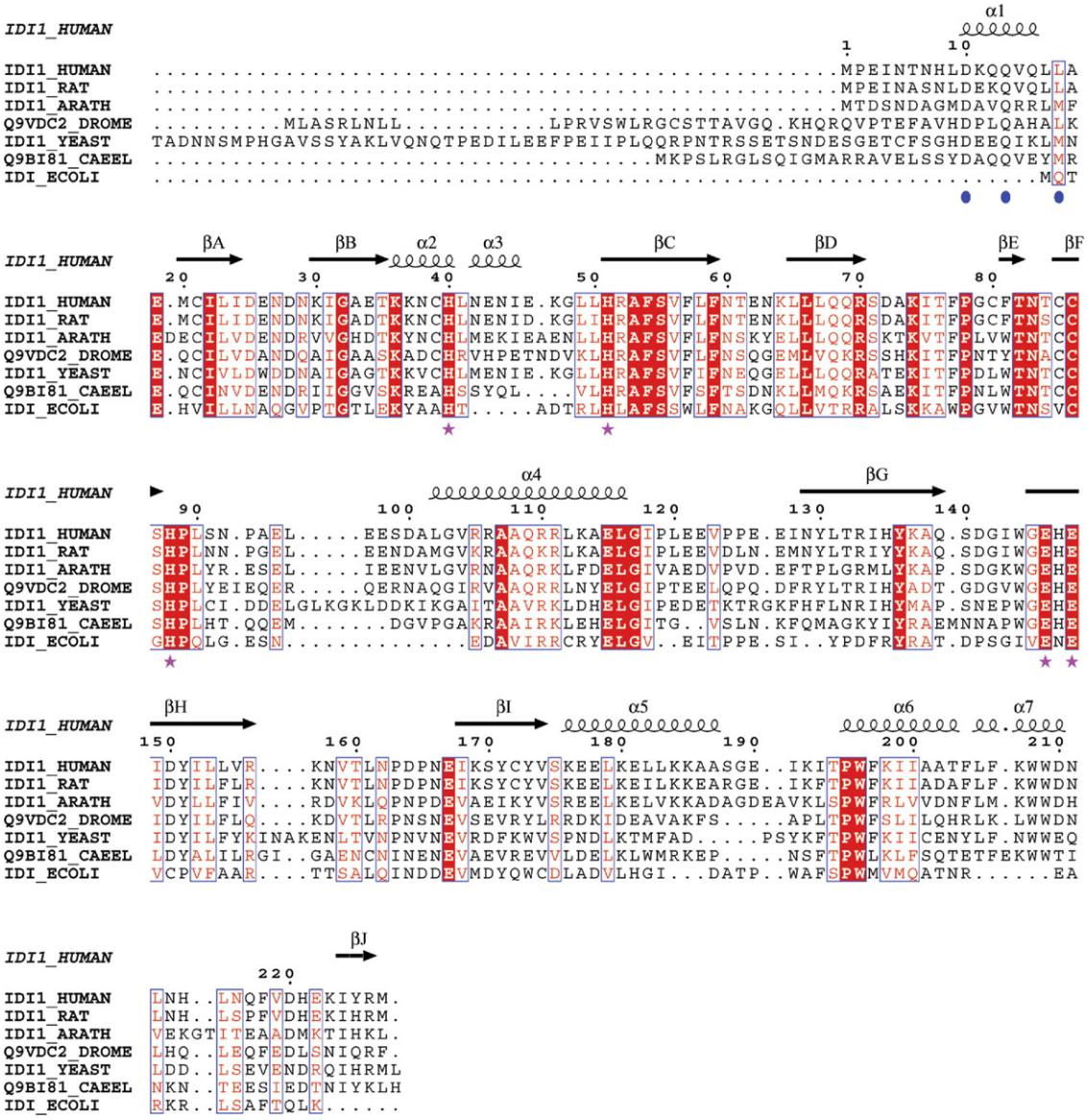

Figure 3. Structure-based sequence alignment of IPP isomerases from human (IDI1_HUMAN), rat (IDI1_RAT), *A. thaliana* (IDI1_ARATH), *Drosophila melanogaster* (Q9VDC2_ DROM E), *Saccharomyces cerevisiae* (IDI1_YEAST), *Caenorhabditis elegans* (Q9BI81_CAEEL) and *E. coli* (IDI_ECOLI). Secondary structure elements in hIPPI2_B are shown above the alignment. Arrows indicate β-strands and coils indicate helices. Strictly conserved and similar residues are boxed and marked with red background and red letters, respectively. Conserved residues binding to the catalysis-required metal ion, H40, H51, H88, E146 and E148 are marked with purple stars under the alignment. D10, Q13 and L17, which contribute to stabilization of the N-terminal α-helix in human IPPI and are highly conserved in eukaryotic IPPIs, are marked with blue circle under the alignment. The multi-sequence alignment was done by T-coffee.[39] The secondary structure of human IPPIB was analyzed by DSSP program.[40] This Figure was prepared using ESPript.[41]

contribute to stabilization of the N-terminal α-helix in human IPPI, are all highly conserved in other eukaryotic IPPIs (Figure 3). This indicates that the unstable N-terminal α-helix in human IPPI, which becomes structurally ordered only upon substrate binding, may also exist in other eukaryotic IPPIs. Previous studies demonstrated lower Michaelis constants (K_m) of eukaryotic IPPIs compared to their bacterial homologs,[25] indicating stronger substrate binding ability for bacterial IPPIs. This unstable N-terminal α-helix, which lies upon the active pocket of eukaryotic IPPIs and may apply some hindrance, could account for their weaker substrate binding ability.

The active site

Based on previous studies of the catalytic mechanism of *E. coli* IPPI, some catalysis required residues could be predicted for human IPPI. These residues include Cys86, Tyr136, Glu148 and Trp196, corresponding to Cys67, Tyr104, Glu116 and Trp161 in *E. coli* IPPI. These four residues are highly conserved in all IPPIs. In human IPPI, Tyr136 and Glu148

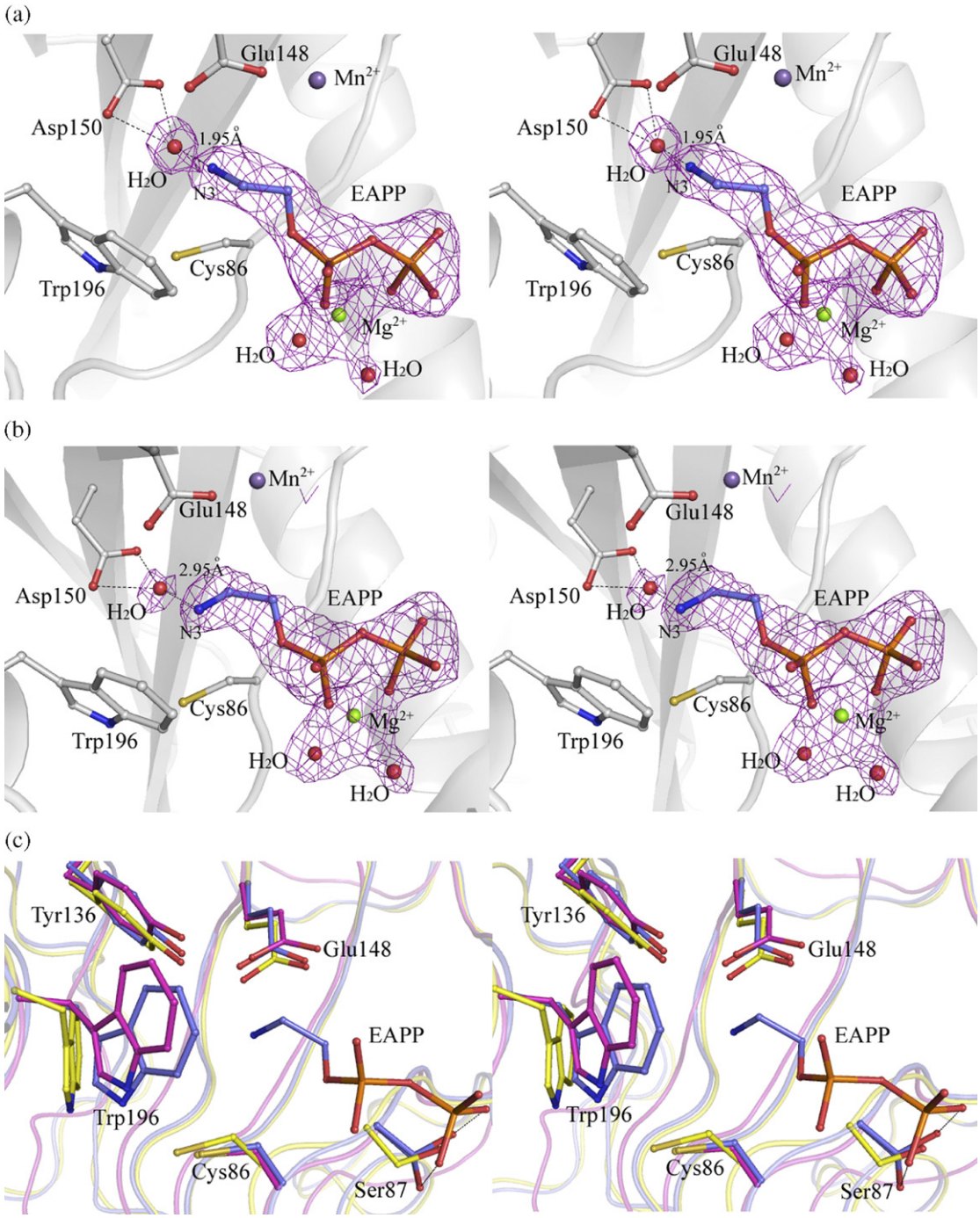

Figure 4. (a) Stereo view of the active site of hIPPI2_A. (b) Stereo view of the active sites of hIPPI2_B. The annealing omit F_o–F_c map (excluding EAPP, Mg^{2+}, two water molecules coordinated to Mg^{2+}, and the water molecule interacting with the N3 atom of EAPP in the refinement model) is colored in purple and contoured at 3.00 σ. Water molecules are shown as red balls. Mg^{2+} is shown as a green ball. The distances between the water molecule and the N3 atom of EAPP are labeled. The pictures clearly demonstrate different conformations of the hydrocarbon tail of EAPP in these two hIPPI2 monomers. (c) Stereo view of superimposition of the active site in hIPPI1 (yellow), hIPPI2_A (blue) and *E.coli* IPPI (PDB code 1NFS) (magenta). Residues are numbered as in human IPPI. Catalytically critical residues Glu148, Tyr136, Trp196 and Cys86 in human IPPI are labeled. The hydrogen bonds between the diphosphate of EAPP and the side-chain of Ser87 in hIPPI2_A are shown as black broken lines. This picture shows the different conformations of Trp196 and the slightly different position of Cys86 in hIPPI1 (yellow) and hIPPI2 (blue).

remain the same conformations in both of the two crystal forms as in *E. coli* IPPI. However, Trp196 shows variable conformations (Figure 4(c)). In hIPPI1, the side-chain of Trp196 is away from the substrate-binding site, forming hydrophobic interactions with Ile134, Ile152 and Ile200, while in hIPPI2, which represents the substrate binding state, the side-chain of Trp196 flips towards the

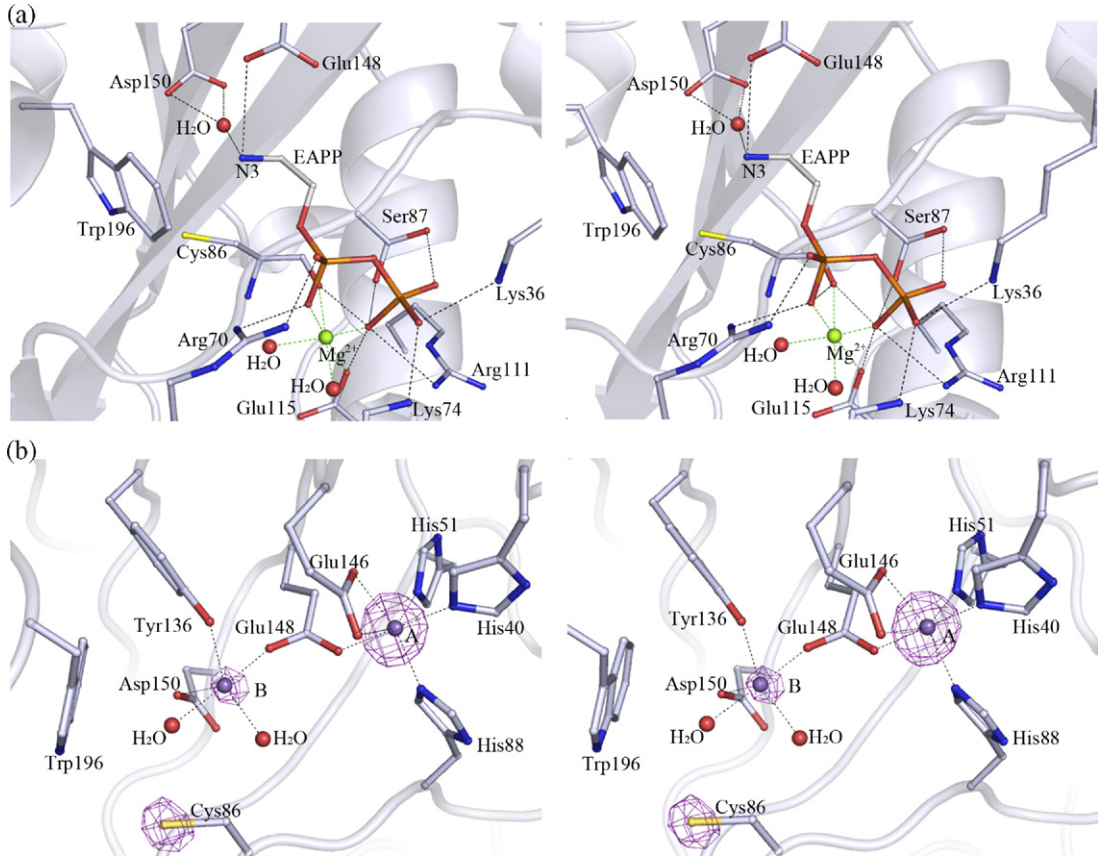

Figure 5. (a) Stereo view of interactions between EAPP and human IPPI (hIPPI2_B). Hydrogen bonds are show as black broken lines. Coordination interactions are show as green broken lines. Water molecules are shown as red balls. Mg^{2+} is shown as a green ball. (b) Stereo view of the inhibition-related and catalysis-required Mn^{2+} binding sites in hIPPI1. Manganese ions are shown as purple balls. Sphere A represents the catalysis-required Mn^{2+}, while Sphere B indicates the inhibition-related Mn^{2+}. Anomalous difference density is colored in purple and contoured at 4.0 σ. Coordination interactions to manganese ions are shown as black broken lines. Two water molecules coordinated to manganese ion B are shown as red balls.

active site. This conformation is similar to Tyr161 in *E. coli* IPPI, in which Tyr161 was proposed to stabilize the carbocation intermediate by a cation–π interaction.[21] Besides, the position of the side-chain of Cys86 in hIPPI2 is nearly the same as that in *E.coli* IPPI (PDB code 1NFS), but is slightly different from that in hIPPI1 (Figure 4(c)).

In hIPPI2, the substrate analog EAPP was identified in the active pocket with the position and orientation similar to *N*,*N*-dimethyl-2-amino-1-ethyl diphosphate (NIPP) bound in *E. coli* IPPI (PDB code 1NFS). Hydrogen bond and coordination interactions are formed between EAPP and the enzyme (Figure 5(a)). The diphosphate group of EAPP is stabilized by forming hydrogen bonds with four highly conserved basic residues Lys36, Arg70, Lys74 and Arg111. An Mg^{2+} binds to two non-bridging oxygen atoms of the diphosphate, two water molecules, one of side-chain oxygen atoms of Glu115 and the carbonyl group of Cys86 with an octahedral geometry. These interactions stabilizing the diphosphate group are similar to those in *E.coli* IPPI. Besides these highly conserved residues, the hydroxyl group of Ser87 (corresponding to Gly68 in *E.coli* IPPI) adopts two conformations and both form hydrogen bonds with the oxygen atoms of the diphosphate group. Several other residues nearby may participate in the stabilization of EAPP *via* indirect hydrogen bonds, including N-terminal residue Glu19. For the amino group of EAPP, interactions are formed between the nitrogen atom of EAPP with the carboxyl oxygen of E148 and with one water molecule. This water molecule is further stabilized by the hydrogen bonds with the two side-chain oxygen atoms of Asp150.

Discussion

Natural substrate analog EAPP is a potential IPPI inhibitor

EAPP is similar to NIPP, a strong inhibitor of *E. coli* IPPI, with the absence of two methyl groups (Figure 1(b)). It is identified in lipopolysaccharide, which is a component of the cell wall outer membrane of Gram-negative bacteria. It seems that EAPP in hIPPI2 comes from the bacteria used for protein expression. The crystals of hIPPI2 were prepared for Se-MAD and the protein was expressed

in the inorganic M9 media containing 2 mM $MgSO_4$. Mg^{2+} is required for IPPI substrate binding, which explains why this substrate analog was only observed in hIPPI2 but not in hIPPI1, since the latter was expressed in the normal LB media. The binding of EAPP to human IPPI should be quite stable because it was not lost during protein purification. EAPP is smaller and simpler than any known IPPI inhibitors. As a natural compound coming from *E. coli* cell wall, EAPP is a potential inhibitor to be developed to a drug that targets human IPPI.

Conformation change of the human IPPI active pocket while EAPP binding

As mentioned before, the conformation of the active site is different in the two hIPPI structures. Compared to hIPPI1, the binding of EAPP to the side-chain of Ser87 causes a slight movement of the main chain between Cys86 and Ser87. The side-chain of the critical residue Cys86 thus moves back a little towards the active pocket (Figure 4(c)). This retreat may result in space enough for the flipping of the Trp196 side-chain. So it can be proposed that in human IPPI, substrate binding would cause conformation change of the active site involving movement of the Cys86 side-chain and flipping of the Trp196 side-chain. This conformation change may result in a catalytically competent state of the active site.

Insight into the catalytic mechanism

In addition to the high conservation between the structures of hIPPI and *E. coli* IPPI active sites, the substrate analog EAPP binds to hIPPI in also a very similar to the way in which NIPP bound in *E. coli* IPPI. These data suggest that the catalytic mechanisms of human and *E. coli* IPPIs would be the same or very similar (Figure 4(c)). Based on the previous studies on *E. coli* IPPI, some critical residues for protonation/deprotonation have been characterized.[21] In *E.coli* IPPI, Glu116 (Glu148 in hIPPI) is proposed to facilitate hydrogen transfer to protonate the carbon-carbon double bond in IPP. Cys67 (Cys86 in hIPPI) acts as a nucleophile that removes a proton from carbocationic intermediate to form a new carbon-carbon double bond between C2 and C3 of IPP. This residue is also proposed to protonate the double bond between C2 and C3 of DMAPP. Cys67 and Glu116 are positioned on the opposite sides of the substrate, which explains the antarafacial stereochemistry of the reaction. However, the original proton donor for IPP is not clear yet. Recent studies indicated that the hydroxyl group of Tyr104 in *E.coli* IPPI (Tyr136 in hIPPI) could not be the proton donor because the Y104F and Y104A *E.coli* IPPI mutants still retain ~1% and ~0.1% of catalytic activities.[11,26] Glu116 in *E.coli* IPPI is important in the protonation step, but whether it is the proton donor for IPP was doubted because Glu116 should be unprotonated even in the absence of substrate.[21,26] Water molecule is a possible proton donor but no well positioned water molecule was found in the active pocket in *E. coli* IPPI structures.[21]

In the structure of human IPPI bound with EAPP (hIPPI2), a water molecule is observed in the active site. There are two monomers per crystallographic asymmetric unit in hIPPI2. Although the diphosphate group of EAPP keeps the same orientation, the conformations of the tail are different (Figure 4(a) and (b)). In each monomer of hIPPI2, the amino group of EAPP interacts with a water molecule. In hIPPI2_B, the distance between the N3 atom and the water molecule is 2.95 Å (Figure 4(b)), which is reasonable for a hydrogen bond. But in hIPPI2_A, the distance is as close as 1.95 Å (Figure 4(a)). It is possible that when IPP binds the enzyme, the distance between this water molecule and the C3–C4 double bond could be close enough for proton transfer and the water molecule could act as the direct proton donor. The side-chains of Tyr136 and Glu148 (human IPPI numbering) could polarize the double bond and make it easier to accept a proton. The polarization by Tyr136 and Glu148 may be essential for the enzymatic activity because the carbon-carbon double bond is difficult to be protonated under normal conditions. The protonation of the double bond results in a carbocation intermediate that could be stabilized by the cation–π interaction with Trp196.

It was found that the eukaryotic IPPIs are more active than *E.coli* IPPI, with k_{cat} values of 1.8~11 s^{-1} for the eukaryotic IPPIs and 0.33 s^{-1} for *E.coli* IPPI.[25] The water molecule proposed as the direct proton donor forms hydrogen bonds with the side-chain of Asp150. It is noticeable that Asp150 in human IPPI is quite conserved in the eukaryotic IPPIs but not in *E.coli* IPPI (Figure 3). The stabilization of the water molecule by Asp150 may be the reason for the increase of the catalytic activities in eukaryotic IPPIs.

The conformation of the hydrocarbon chain of EAPP in hIPPI2_B is different from that in hIPPI2_A. In hIPPI2_B, the C2 atom of EAPP seems to be closer to the thiol group of Cys86 than that in hIPPI2_A (Figure 4(a) and (b)). This conformation may represent the way DMAPP bound to the enzyme in which it would be easier for the thiol group of Cys86 to protonate the double bond between the C2 and C3 atoms. The water molecule hydrogen bonding with the N3 atom of EAPP in hIPPI2_B may participate in the deprotonation process. The different conformations of IPP and DMAPP in which they bind the enzyme may account for the reversibility of the reaction.

Inhibition of high Mn^{2+} concentration for human IPPI

Human IPPI activity is enhanced by increasing concentration of Mn^{2+} but decreased sharply at higher Mn^{2+} concentrations over 100 μM.[27] In the structure of hIPPI1, a total of eight Mn^{2+} were found binding with the protein. Besides the one required

for catalysis, another ion is also bound inside the catalytic pocket, coordinated to Glu148, Tyr136, Aps150 and two water molecules with a distorted bi-pyramid geometry (Figure 5(b)). This Mn^{2+} occupies the space for the substrate and prevents the hydrogen transfer facilitated by Glu148. Therefore, it may deprive the activity of human IPPI. However, the binding affinity for the second Mn^{2+} may be lower than that for the catalytic Mn^{2+}, which is supported by its low occupancy of 0.2. Therefore it could not interfere with the substrate binding at a low concentration of Mn^{2+}. On the other hand, this inhibition is not observed for *E. coli* IPPI,[27] in which Cys118 corresponds to Asp150 of human IPPI. The shorter side-chain of cysteine may result in abolition of the second Mn^{2+} binding ability.

Materials and Methods

Gene cloning, expression and protein purification

The complete human IPP isomerase cDNA was cloned from human brain cDNA library (Clontech) by PCR using 5′ CAGTCCATATGCCTGAAATAAACA 3′ and 5′ CACTGCGGCCGCTCACATTCTGTATATTTCTC 3′ as primers. The amplified DNA was cloned into vector p28, which was derived from pET28b (Novagen). The clone was sequenced and a mutation was identified, resulting in a mutant K157M. Based on the hIPPI structures, such mutated residue is located on the surface of the enzyme and far away from the active site. The mutant $hIPPI_{K157M}$ was used in our crystallogrphy studies. Recombinant human IPP isomerase was expressed in *E.coli* BL21 (DE3) with six histidine residues at the N terminus. *E.coli* cells were grown in LB media for normal recombinant protein expression and in inorganic M9 media containing 40 mg/l selenomethione (Se-Met), 2 mM $MgSO_4$, 0.1 mM $CaCl_2$ and 0.05 μM $FeSO_4$ for selenomethionyl protein expression. Bacterial cells were grown in LB media with kanamycin sulfate (50 μg/ml) at 20 °C, induced overnight with 0.5 mM IPTG, and harvested by centrifugation. The cell pellet was re-suspended in 20 mM Tris-HCl (pH 7.5), 200 mM NaCl, 1 mM PMSF followed by sonication on ice. The lysate was clarified by centrifugation and the supernatant was further purified with a Nickel Chelating Sepharose™ Fast Flow (Amersham Biosciences) column followed by gel filtration chromatography with Superdex™ 75 (Amersham Biosciences). Final concentration of both native and Se-Met-substituted hIPPI protein was 15 mg/ml, determined by Bio-Rad Protein Assay. Protein purity and molecular mass (~26 kDa) were verified by SDS-PAGE.

Crystallization and data collection

Initial crystallization conditions for recombinant human IPP isomerase were screened using Crystal Screen kits I and II from Hampton research by hanging-drop vapor diffusion method at 4 °C. The high quality crystals of native hIPPI were grown under condition containing 0.4 M $MnCl_2$, 0.1 M sodium cacodylate (pH 6.5) and 20% (w/v) PEG8000 within seven days (hIPPI1). The Se-Met derivative crystals (hIPPI2) were grown under condition containing 0.2 M magnesium acetate, 0.1 M sodium cacodylate (pH 6.5) and 20% PEG8000. Diffraction data of the two different crystal forms were collected at a Rigaku R-AXIS IV^{++} imaging-plate system with a Rigaku FRE Cu rotating-anode generator in Institute of Biophysics, Chinese Academy of Sciences, and processed with DENZO and SCALEPACK.[28]

Structure determination and refinement

The crystal grown with 0.4 M $MnCl_2$ was used for phasing by the SAD method. SHELXD[29] was used to find three Mn^{2+}. Heavy atom refinement and phase calculation were performed by autoSHARP.[30] Automatic model building was performed by ARP/wARP[31] and the final model was refined to 1.6 Å resolution by Refmac5.[32] TLS refinement[33] was performed in Refmac5 with 15 TLS groups suggested by TLSMD.[34] Iterative manual adjustments of the model were finished in Coot.[35] The structure of Se-Met hIPPI was solved by molecular replacement using Molrep[36] and the model was refined to 2.0 Å resolution by Refmac5. EAPP, metal ions and the active site water molecule were identified at the latest stage of refinement according to a series of omit-annealing electron density maps and anomalous signal analysis. The original coordinates of EAPP were obtained from the HIC-Up database† and the EAPP molecule was manually fitted into the omit F_o–F_c map. The topology and parameter file of EAPP used for Refmac5 was made by PRODRG‡.[37] The stereochemical qualities of the final models were checked by PROCHECK.[38]

Protein Data Bank accession code

The atomic coordinates have been deposited in the RCSB Protein Data Bank, with the accession code 2DHO for hIPPI1 and 2I6K for hIPPI2.

Acknowledgements

This work is supported by National Funding for Talent Youth (Grant No. 30225015), the 973 Program of the Ministry of Science and Technology (No. 2004CB720008), the National Natural Science Foundation of China (Grant No. 10490193) and the Chinese Academy of Sciences (KSCX1-YW-R-61). We thank Mr Yi Han in the Institute of Biophysics for diffraction data collection.

References

1. Sacchettini, J. C. & Poulter, C. D. (1997). Creating isoprenoid diversity. *Science*, **277**, 1788–1789.
2. Edwards, P. A. & Ericsson, J. (1999). Sterols and isoprenoids: signaling molecules derived from the cholesterol biosynthetic pathway. *Annu. Rev. Biochem.* **68**, 157–185.
3. Winter-Vann, A. M. & Casey, P. J. (2005). Post-prenylation-processing enzymes as new targets in oncogenesis. *Nature Rev. Cancer*, **5**, 405–412.

† http://xray.bmc.uu.se/hicup/
‡ http://davapc1.bioch.dundee.ac.uk/programs/prodrg/

4. Popjak, G. (1970). In *Natural Substances Formed Biologically from Mevalonic Acid* (Goodwin, T. W., ed), Academic Press, New York.
5. Agranoff, B. W., Eggerer, H., Henning, U. & Lynen, F. (1960). Biosynthesis of terpenes. VII. Isopentenyl pyrophosphate isomerase. *J. Biol. Chem.* **235**, 326–332.
6. Rohdich, F., Bacher, A. & Eisenreich, W. (2004). Perspectives in anti-infective drug design. The late steps in the biosynthesis of the universal terpenoid precursors, isopentenyl diphosphate and dimethylallyl diphosphate. *Bioorg. Chem.* **32**, 292–308.
7. Chen, Z. W. (2005). Immune regulation of gammadelta T cell responses in mycobacterial infections. *Clin. Immunol.* **116**, 202–207.
8. Cairo, C., Propp, N., Hebbeler, A. M., Colizzi, V. & Pauza, C. D. (2005). The Vgamma2/Vdelta2 T-cell repertoire in *Macaca fascicularis*: functional responses to phosphoantigen stimulation by the Vgamma2/Jgamma1.2 subset. *Immunology*, **115**, 197–205.
9. Rojas, R. E., Torres, M., Fournie, J. J., Harding, C. V. & Boom, W. H. (2002). Phosphoantigen presentation by macrophages to mycobacterium tuberculosis-reactive Vgamma9Vdelta2+T cells: modulation by chloroquine. *Infect. Immun.* **70**, 4019–4027.
10. Cheng, F. & Oldfield, E. (2004). Inhibition of isoprene biosynthesis pathway enzymes by phosphonates, bisphosphonates, and diphosphates. *J. Med. Chem.* **47**, 5149–5158.
11. Wouters, J., Yin, F., Song, Y., Zhang, Y., Oudjama, Y., Stalon, V. *et al.* (2005). A crystallographic investigation of phosphoantigen binding to isopentenyl pyrophosphate/dimethylallyl pyrophosphate isomerase. *J. Am. Chem. Soc.* **127**, 536–537.
12. Cornforth, J. W., Cornforth, R. H., Popjak, G. & Yengoyan, L. (1966). Studies on the biosynthesis of cholesterol. XX. Steric course of decarboxylation of 5-pyrophosphomevalonate and of the carbon to carbon bond formation in the biosynthesis of farnesyl pyrophosphate. *J. Biol. Chem.* **241**, 3970–3987.
13. Street, I. P., Christensen, D. J. & Poulter, C. D. (1990). Hydrogen exchange during the enzyme-catalyzed isomerization of isopentenyl diphosphate and dimethylallyl diphosphate. *J. Am. Chem. Soc.* **112**, 8577–8578.
14. Muehlbacher, M. & Poulter, C. D. (1988). Isopentenyldiphosphate isomerase: inactivation of the enzyme with active-site-directed irreversible inhibitors and transition-state analogues. *Biochemistry*, **27**, 7315–7328.
15. Reardon, J. E. & Abeles, R. H. (1986). Mechanism of action of isopentenyl pyrophosphate isomerase: evidence for a carbonium ion intermediate. *Biochemistry*, **25**, 5609–5616.
16. Lu, X. J., Christensen, D. J. & Poulter, C. D. (1992). Isopentenyl-diphosphate isomerase: irreversible inhibition by 3-methyl-3,4-epoxybutyl diphosphate. *Biochemistry*, **31**, 9955–9960.
17. Street, I. P., Coffman, H. R., Baker, J. A. & Poulter, C. D. (1994). Identification of Cys139 and Glu207 as catalytically important groups in the active site of isopentenyl diphosphate:dimethylallyl diphosphate isomerase. *Biochemistry*, **33**, 4212–4217.
18. Durbecq, V., Sainz, G., Oudjama, Y., Clantin, B., Bompard-Gilles, C., Tricot, C. *et al.* (2001). Crystal structure of isopentenyl diphosphate:dimethylallyl diphosphate isomerase. *EMBO J.* **20**, 1530–1537.
19. Wouters, J., Oudjama, Y., Ghosh, S., Stalon, V., Droogmans, L. & Oldfield, E. (2003). Structure and mechanism of action of isopentenylpyrophosphate-dimethylallylpyrophosphate isomerase. *J. Am. Chem. Soc.* **125**, 3198–3199.
20. Wouters, J., Oudjama, Y., Stalon, V., Droogmans, L. & Poulter, C. D. (2004). Crystal structure of the C67A mutant of isopentenyl diphosphate isomerase complexed with a mechanism-based irreversible inhibitor. *Proteins: Struct. Funct. Genet.* **54**, 216–221.
21. Wouters, J., Oudjama, Y., Barkley, S. J., Tricot, C., Stalon, V., Droogmans, L. & Poulter, C. D. (2003). Catalytic mechanism of *Escherichia coli* isopentenyl diphosphate isomerase involves Cys-67, Glu-116, and Tyr-104 as suggested by crystal structures of complexes with transition state analogues and irreversible inhibitors. *J. Biol. Chem.* **278**, 11903–11908.
22. Lee, S. & Poulter, C. D. (2006). *Escherichia coli* type I isopentenyl diphosphate isomerase: structural and catalytic roles for divalent metals. *J. Am. Chem. Soc.* **128**, 11545–11550.
23. Paton, V. G., Shackelford, J. E. & Krisans, S. K. (1997). Cloning and subcellular localization of hamster and rat isopentenyl diphosphate dimethylallyl diphosphate isomerase. A PTS1 motif targets the enzyme to peroxisomes. *J. Biol. Chem.* **272**, 18945–18950.
24. Carrigan, C. N. & Poulter, C. D. (2003). Zinc is an essential cofactor for type I isopentenyl diphosphate: dimethylallyl diphosphate isomerase. *J. Am. Chem. Soc.* **125**, 9008–9009.
25. Hahn, F. M., Hurlburt, A. P. & Poulter, C. D. (1999). *Escherichia coli* open reading frame 696 is idi, a nonessential gene encoding isopentenyl diphosphate isomerase. *J. Bacteriol.* **181**, 4499–4504.
26. de Ruyck, J., Durisotti, V., Oudjama, Y. & Wouters, J. (2006). Structural role for TYR-104 in *Escherichia coli* isopentenyl-diphosphate isomerase: site-directed mutagenesis, enzymology and protein crystallography. *J. Biol. Chem.* **281**, 17864–17869.
27. Hahn, F. M., Xuan, J. W., Chambers, A. F. & Poulter, C. D. (1996). Human isopentenyl diphosphate: dimethylallyl diphosphate isomerase: overproduction, purification, and characterization. *Arch. Biochem. Biophys.* **332**, 30–34.
28. Otwinowski, Z. M. W. (1997). Processing of X-ray diffraction data collected in oscillation mode. *Methods Enzymol.* **276**, 307–326.
29. Schneider, T. R. & Sheldrick, G. M. (2002). Substructure solution with SHELXD. *Acta Crystallog. sect. D*, **58**, 1772–1779.
30. Vonrhein, C., Blanc, E., Roversi, P. & Bricogne, G. (2006). Automated structure solution with autoSHARP. In *Crystallographic Methods* (Doublie, S., ed), pp. 215–230, Humana Press, Totowa, NJ.
31. Perrakis, A., Morris, R. & Lamzin, V. S. (1999). Automated protein model building combined with iterative structure refinement. *Nature Struct. Biol.* **6**, 458–463.
32. Murshudov, G. N., Vagin, A. A. & Dodson, E. J. (1997). Refinement of macromolecular structures by the maximum-likelihood method. *Acta Crystallog. sect. D*, **53**, 240–255.
33. Winn, M. D., Murshudov, G. N. & Papiz, M. Z. (2003). Macromolecular TLS refinement in REFMAC at moderate resolutions. *Methods Enzymol.* **374**, 300–321.
34. Painter, J. & Merritt, E. A. (2005). A molecular viewer for the analysis of TLS rigid-body motion in macromolecules. *Acta Crystallog. sect. D*, **61**, 465–471.
35. Emsley, P. & Cowtan, K. (2004). Coot: model-building tools for molecular graphics. *Acta Crystallog. sect. D*, **60**, 2126–2132.
36. Vagin, A. T. (1997). MOLREP: an automated program for molecular replacement. *J. Appl. Crystallog.* **30**, 1022–1025.

37. Schuttelkopf, A. W. & van Aalten, D. M. (2004). PRODRG: a tool for high-throughput crystallography of protein-ligand complexes. *Acta Crystallog. sect. D*, **60**, 1355–1363.
38. Laskowski, R. A., MacArthur, M. W., Moss, D. S. & Thornton, J. M. (1993). PROCHECK: a program to check the stereochemical quality of protein structures. *J. Appl. Crystallog.* **26**, 283–291.
39. Notredame, C., Higgins, D. G. & Heringa, J. (2000). T-Coffee: a novel method for fast and accurate multiple sequence alignment. *J. Mol. Biol.* **302**, 205–217.
40. Kabsch, W. & Sander, C. (1983). Dictionary of protein secondary structure: pattern recognition of hydrogen-bonded and geometrical features. *Biopolymers*, **22**, 2577–2637.
41. Gouet, P., Courcelle, E., Stuart, D. I. & Metoz, F. (1999). ESPript: analysis of multiple sequence alignments in PostScript. *Bioinformatics*, **15**, 305–308.

Edited by I. Wilson

(Received 1 September 2006; received in revised form 24 October 2006; accepted 26 October 2006)
Available online 3 November 2006